Macromolecular Materials and Engineering
Open Access
www.mame-journal.de

Fabrication and In Vitro Characterization of Polycaprolactone/Graphene Oxide/Collagen Nanofibers for Myocardial Repair

Sema Seren Karapehlivan, Mehmet Necati Danisik, Zekiye Akdag, Elif Nur Yildiz, Oseweuba Valentine Okoro, Lei Nie, Amin Shavandi, Songul Ulag, Ali Sahin, Fatih Dumludag, and Oguzhan Gunduz**

This study is focused on fabricating tissue-engineered electrospun nanofibers that contain polycaprolactone (PCL), graphene oxide (GO), and collagen (COL) to get an alternative treatment for cardiac injuries. GO (1.5 wt%) is used to support the contraction-elongation of cardiomyocytes by improving electrical stimulation. The COL (1, 3, and 5 wt%) is the main component of the myocardial extracellular matrix have led to their frequent use in cardiac tissue engineering (CTE). The scanning electron microscope (SEM) images show the homogeneous and bead-free morphologies of the nanofibers. Adding a high amount (3% and 5%) of COL decreases the tensile strength value of 17% PCL/1.5% GO nanofiber. 3-(4,5-Dimethylthiazol-2-yl)-2,5-Diphenyltetrazolium Bromide (MTT) assay demonstrates that the COL addition increases cell viability compared to that in 17% PCL/1.5% GO nanofibers on the third day. The response of the nanofibers to alternating current (AC) signal is studied between the frequencies 40 and 10^5 Hz. The direct current (DC) conductivity values of the films are determined to be between 1.10^{-10} and 6.10^{-10} S m^{-1} at 25 °C. The AC conductivity values show frequency-dependent behavior. Among the PCL/GO-based electrospun nanofibers, 17% PCL/1.5% GO/5% COL nanofiber shows greater DC and AC conductivity than 17% PCL/1.5% GO nanofiber.

1. Introduction

Myocardial infarction (MI) happens when the cardiac muscle tissue is damaged and replaced by scar tissue.[1] Therefore, MI ranks first among cardiovascular diseases that cause loss of functionality and even death.[2] Heart transplantation is recognized as a common and active treatment recommended by cardiologists.[3] However, this treatment method has many limitations, such as insufficient donors and immune rejection risk. Similarly, the method in which the damaged area is directly treated with cells was insufficient to provide long-term treatment, even though it could restore its former functionality to the heart.[4] Because a large number of cardiomyocytes cannot survive after stem cell transfer[3,5] and cannot participate in myofunction, in some cases, surviving cells cannot integrate with surrounding tissues by failing to establish appropriate intercellular electrical connections.[6] Recently,

S. S. Karapehlivan, M. N. Danisik, Z. Akdag, E. N. Yildiz, S. Ulag, O. Gunduz
Center for Nanotechnology and Biomaterials Application & Research (NBUAM)
Marmara University
Istanbul 34722, Turkey
E-mail: songul.ulag@marmara.edu.tr; ucemogu@ucl.ac.uk

S. S. Karapehlivan, M. N. Danisik, S. Ulag, O. Gunduz
Department of Metallurgical and Materials Engineering, Faculty of Technology
Marmara University
Istanbul 34722, Turkey

Z. Akdag
Department of Metallurgical and Materials Engineering, Institute of Pure and Applied Sciences
Marmara University
Istanbul 34722, Turkey

E. N. Yildiz
Department of Molecular Biology and Genetics, Faculty of Arts and Sciences
Yildiz Technical University
Istanbul 34220, Turkey

O. V. Okoro, A. Shavandi
BioMatter unit - École Polytechnique de Bruxelles
Université Libre de Bruxelles (ULB)
Avenue F.D. Roosevelt, 50 - CP 165/61, Brussels 1050, Belgium

L. Nie
College of Life Sciences
Xinyang Normal University (XYNU)
Xinyang 464000, China

The ORCID identification number(s) for the author(s) of this article can be found under https://doi.org/10.1002/mame.202300189

DOI: 10.1002/mame.202300189

tissue engineering and regenerative medicine have provided a scaffold-like structure to support cardiac cell proliferation, communication, and function or an effective strategy through substrate delivery for restoring cardiac tissue and its functionality.[7] The designed structures tend to mimic the composition, flexibility, and micro/nano morphology of the extracellular matrix of native cardiac muscle tissue. Electrical conductivity, one of the critical properties of cardiac muscle tissue, is responsible for proper cardiac functionality and self-healing. An electroactive network between cardiac muscle tissue cells provides their essential communication. If such electrical communication is lost or damaged, it will cause a significant reduction in cardiac function by disrupting the transmitted cell-cell electrical signals.[8] Therefore, considering the electrical conductivity properties of cardiac scaffolds or substrates appears to be an essential issue in cardiac muscle tissue regeneration. The cardiac muscle tissue patch is designed to promote myocardial regeneration in patients suffering from heart attack side effects.[9] These scaffolds are often designed as a patch of synthetic, natural, and synthetic/natural polymeric biomaterials. Electrospinning is the most common method used to fabricate these cardiac scaffolds. It is the process of using high-voltage electricity for manufacturing fibers with diameters ranging from nanoscale to microscale. Among the fabrication methods, electrospinning is easy to process and cheap.

In addition, surface properties, porosity status, fiber diameter, and type, as well as mechanical properties of the produced fibers, can be controlled by electrospinning.[10] Furthermore, the vast potential of fiber production makes electrospinning very suitable for tissue engineering. It is a widely used method that allows polymers such as polycaprolactone (PCL), polylactic acid (PLA),[11] collagen (COL), and aggregates such as graphene oxide (GO), and carbon nanotubes (CNT) to be used together and used in the composite form.[12] On the other hand, it is disadvantageous compared to nozzle-free techniques in creating only one fiber from a single needle.[13] However, in this study, the classical electrospinning method was used since large-scale production was not carried out.

Non-polymeric aggregates such as graphene[14] and CNT[15] play a role in stimulating cellular communication in cardiac tissue engineering (CTE). In addition, these materials have essential properties such as improving mechanical properties, angiogenesis potential, and electroactivity.[16] GO, an oxidized structure of doped graphene, has chemical, physical, and mechanical properties rising from its versatile and unique form. Common applications of GO include tissue engineering, gene therapy, and biosensors.[14] Regarding dose, size, and functionality-dependent cytotoxicity,[17] in vitro and in vivo use of GO can be controlled.[18] In addition to biocompatibility, GO attracts attention with its electroactivity,[19] antibacterial,[20] antioxidative,[21] and angiogenic properties, which are needed in the cardiac tissue regeneration process. GO supports the contraction-elongation of cardiac cells by providing electrical stimulation. Recent research has demonstrated that conductive nanofibers are favored over their insulating polymer equivalents for CTE applications. Due to their exceptional physical qualities, like their high mechanical strength and distinctive electrical conductivity, carbon nanomaterials, particularly CNT and graphene, are regarded as viable reinforcing materials for such applications.[22] Pınar et al. produced a composite electrospun nanofiber containing GO and PCL using the electrospinning technique. Cell culture tests in this study showed that the composite form of PCL with GO increased cellular proliferation, cell attachment, and neuronal differentiation.[17] In the study performed by Shin et al., myocardial tissue structures were designed based on gelatin methacryloyl hybrid hydrogels containing reduced graphene oxide (rGO), and they observed that the addition of rGO increased both electrical conductivity and mechanical strength.[22]

PCL is a biocompatible polymer widely used in biomedical and cardiovascular applications, notably.[23] PCL is structured in the form of nano/microfiber mats. Its bio-inertness, large surface area, high porosity, and interconnected pores make PCL a great candidate for biomedical applications.[24] Wu et al. designed a conductive fiber hybrid scaffold of PCL, silk fibroin (SF), and CNT to enable cardiac tissue regeneration by mimicking the anisotropic cardiac structure.[25] It was reported that the produced hybrid scaffold increased the attachment and maturation of the cardiomyocytes to the damaged area. COL is a natural polymer widely used in biosensors, tissue engineering, and biomedical applications.[26] ≈75–80% of the structure of the myocardial extracellular matrix is COL, making it an excellent option for CTE. Cardiac fibroblasts synthesize COL. This gives cardiac tissue flexibility and contributes to its interaction with integrins that mediate cellular adhesion.[27] COL exhibits high biocompatibility, but its scaffold applications are limited due to its weak mechanical properties. The limitations of COL have been tried to overcome by using COL as an active ingredient in the hybrid biomaterials.[28] A hybrid hydrogel study by Roshanbinfar et al. proved that COL provides electrical conductivity and maturation of cardiomyocytes on neonatal rat cardiomyocytes.[29] In this study, PCL/GO-based COL-doped nanofibers were designed and fabricated using the electrospinning method for. The nanofiber structure was created with PCL due to its high biocompatibility in CTE. In the developed structure, GO provided electroconductivity, while COL increased cell growth and proliferation. It is unique in that there are no studies on cardiac tissue applications involving the combination of PCL, GO, and COL.

2. Experimental Section

2.1. Materials

PCL (M_w=80.000 g mol^{-1}), phosphate buffer saline (PBS, pH=7.4), and Tween-80 (surfactant) were obtained from Sigma-Aldrich, UK. Chloroform and dimethylformamide (DMF) were purchased from Merck KGaA, Germany. The GO powder was prepared with Hummers' method[30] (10–20 layers, thickness of 4.2 nm). COL type I was purchased from Collagen Arge company.

A. Sahin
Genetic and Metabolic Diseases Research and Investigation Center
Marmara University
Istanbul 34854, Turkey
F. Dumludag
Department of Physics, Faculty of Science
Marmara University
Istanbul 34722, Turkey

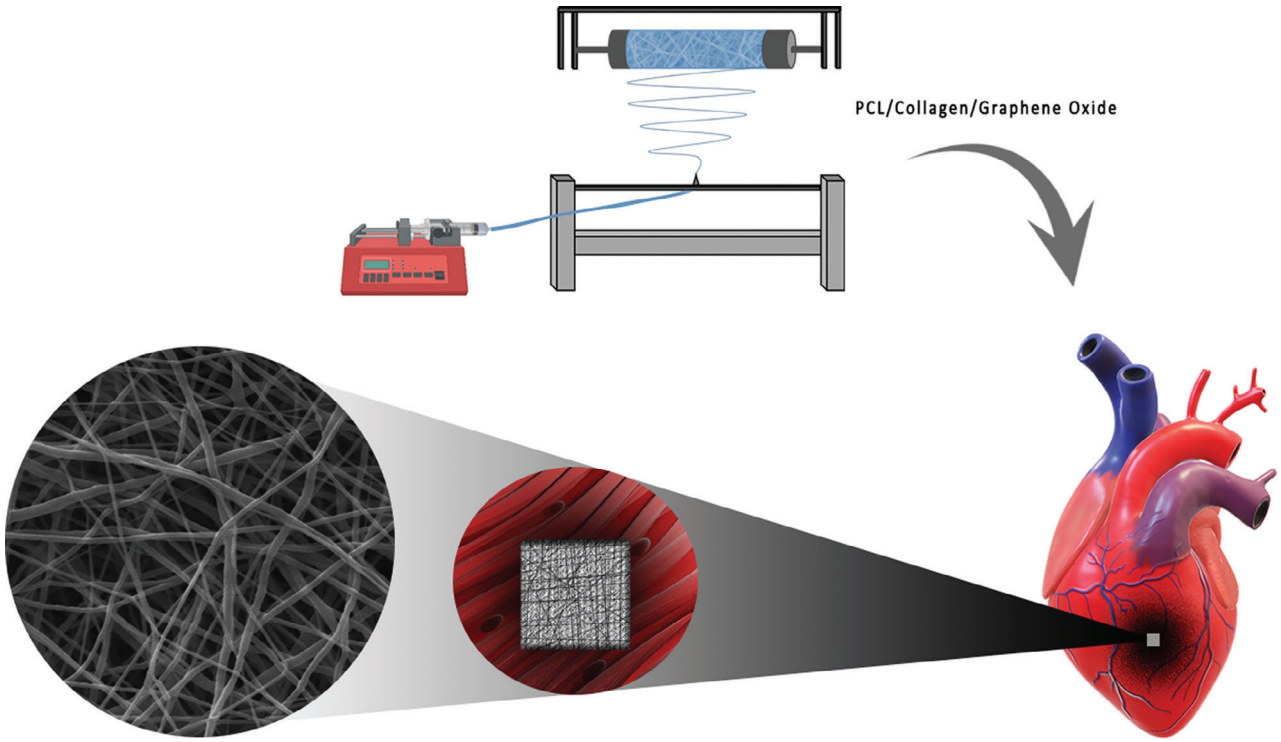

Figure 1. The schematic illustration of the experimental setup.

2.2. Preparation of the Solutions

Initially, 17% PCL was placed in 20 mL of DMF/chloroform (25:75) anhydrous solvent mixture and completely dissolved using a magnetic stirrer for 1 h. Then, 1.5% GO was added into the 17% PCL solution, and it was utterly mixed for 2 h at room temperature using a magnetic stirrer.[19] Finally, 1%, 3%, and 5% COL solutions (acetic acid/distilled water solution which contains the 2% acetic acid ratio) were added separately to the obtained 17% PCL/1.5% GO solution and mixed for 1 h using a stirrer. They were suitable for electrospinning after the COL was utterly dispersed.

2.3. Fabrication of the Electrospun Nanofibers

After the preparation of the solutions, electrospun nanofibers were produced by the electrospinning method (**Figure 1**). In the electrospinning device (NS24, Inovenso Co., Istanbul, Turkey), important parameters such as the distance between the collector and needle, voltage, and flow rate values of the solutions were optimized during the experiment. The amount of solution was provided by the syringe pump (NS24, Inovenso Co., Istanbul, Turkey). The needle has an outer diameter of 0.163 mm, and the 10 mL of syringe was used. To form the smoothest fibers according to the content of the solution, the distance between the needle tip and the collector was fixed at 200 mm, and the temperature was set at room temperature. On the other hand, the flow rate was changed from 0.3 to 1 mL h^{-1}, and the voltage between the needle and collector required for fiber formation varied between 25.0 and 27.0 kV.

2.4. Characterization of the Fibers

2.4.1. Fourier Transform Infrared Spectroscopy

The chemical properties of all electrospun scaffolds were analyzed using Fourier transform infrared spectroscopy (FT-IR) (Jasco, FT/IR 4700, Pfungstadt, Germany). Measurements were performed between 4000 and 400 cm^{-1} wavelength with 32 scans and 4 cm^{-1} resolution value.

2.4.2. Scanning Electron Microscope

SEM (EVA MA 10, ZEISS, San Diego, CA, USA) was used to examine the morphologies of the electrospun nanofibers. Before taking the SEM image, the nanofibers were coated with a Au using a sputter coater (SC7620, Quorum, Lewes, UK) for 120 s. A voltage of 10 kV was applied for analysis, and various magnifications were used for scans. After obtaining SEM images, 100 fibers were selected randomly, and their diameters were determined using Olympus AnalySIS software (Tokyo, Japan).

2.4.3. Differential Scanning Calorimeter (DSC)

DSC (Shimadzu, Japan) was used to examine and interpret the produced electrospun fibers in terms of their thermal transition points, such as melting temperature (T_m) and glass transition temperature (T_g). To obtain the results, the samples were exposed to a heating rate of 10 °C min^{-1}, and the measurements were analyzed in the range of 25 to 350 °C.

2.4.4. X-Ray Diffraction (XRD)

The crystalline structures of electrospun fibers were analyzed using XRD(Shimadzu-6100, Japan). Cu (=1.54060 A°) was used as an X-ray source. The scan range was changed from 10° to 90°, and the scan speed was altered to 2° min^{-1}.

2.4.5. Mechanical Analysis

The mechanical properties of nanofibers were tested with vertical axis tensile testing (Shimadzu Corporation, EZ-LX, Kyoto, Japan). Before starting the analysis, three samples were prepared from each group, which were determined according to the standards and had an average width of 10 mm and a height of 50 mm. The thickness values of all prepared nanofibers were measured using a digital micrometer (Mitutoyo MTI Corp., USA). During the measurement, the test speed was kept at 5 mm min^{-1}. The Young's modulus values of the nanofibers were calculated from the slope of the stress versus strain graph, which is described by Hooke's law.

2.4.6. Swelling Properties of the Fibers

The swelling properties of the nanofibers were investigated in vitro conditions. The PBS with pH 7.4 was used for the swelling test. Equal amounts of weighed nanofibers were placed in Eppendorf tubes containing 1 mL of PBS. Then, Eppendorf tubes were placed in a shaker (BIOSAN TS-100) at 37 °C with 300 rpm. At the end of 24 h, each sample was weighed after being kept on coarse filter paper. The same PBS was used throughout the test. This process continued for 15 days. The swelling rate (S) was calculated using Equation (1), where W_0 is the initial weight, and W_w is the wet weight.

$$S = \frac{W_W - W_0}{W_0} \times 100 \quad (1)$$

2.4.7. Cell Culture Studies

Before evaluating the biocompatibility properties of the electrospun fibers, they were cut in equal sizes to fit the 96-well plate using a circular mold with a diameter of 5 mm. The fibers were then exposed to ultraviolet (UV) light for 2–4 h for sterilization. Dulbecco's Modified Eagle Medium (DMEM) cell culture media supplemented with fetal bovine serum (FBS), penicillin/streptomycin solution, and L-glutamine were used throughout the experiment. The cardiomyocytes (5×10^3 cells $well^{-1}$) were obtained from the American-type culture collection (ATCC, H9c2(2-1), CRL-1446, Manassas, VA, USA). The sterilized nanofibers were incubated for 1 week in an incubator at 37 °C with a 5% CO_2 atmosphere for MTT (3-(4,5-dimethylthiazol-2-yl)−2,5-diphenyl-2H-tetrazolium bromide) assay. The viability of cardiomyocytes on the nanofibers was determined quantitatively by the MTT assay measurements made at the end of the first, third, and seventh days. After incubation, all media in the wells was removed, and the nanofibers were rinsed three times

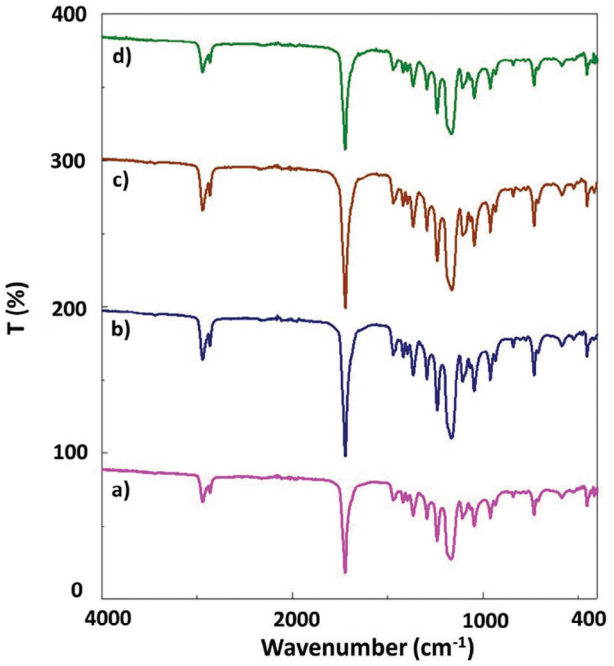

Figure 2. FT-IR spectrums of the a) 17% PCL/1.5% GO, b) 17% PCL/1.5% GO/1% COL, c) 17% PCL/1.5% GO/3% COL, and d) 17% PCL/1.5% GO/5% COL nanofibers.

with PBS solution. 90 µL fresh medium and 10 µL MTT solution (5 mg mL^{-1} in PBS solution) were added to the freshly washed nanofibers and incubated for 3 h. After discarding the medium on the nanofibers, the nanofibers were removed, and the wells were cleaned. After adding 100 µL Dimethyl sulfoxide (DMSO) to dissolve the formazan crystals, the nanofibers were incubated for 1 h. The medium was removed from the wells, and absorbance values were measured at 540 nm with a microplate reader. The test was performed three times, and the average of the results was taken as the final result.

The attachment of cardiomyocytes to the nanofibers was investigated by 4',6-diamidino-2-phenylindole (DAPI) staining. The growth medium was discarded at the end of 1, 3, and 7 days, and the nanofibers were rinsed with PBS. Then, the nanofibers were fixed with 4% formaldehyde for 30 min at room temperature. The washing step with PBS was repeated. To stain the cell nuclei, 1 µg mL^{-1} DAPI was added to each sample at room temperature for 20 min. Then, the DAPI solution was removed, and the nanofibers were placed on a slide and covered with a coverslip. The inverted fluorescence microscope (Leica) was used to observe the cells on the fibers. The morphologies of attached cardiomyocytes on the nanofibers were investigated with SEM. At the end of 1, 3, and 7 days, the growth medium was removed, and all nanofibers were fixed with 4% glutaraldehyde. It was then dehydrated with serial dilutions of ethanol and dried at room temperature.

2.4.8. The Sample Preparation for Electrical Measurements

To measure DC and AC electrical parameters such as conductivity, metal electrodes were deposited on both sides of the thick films of the PCL/GO-based electrospun nanofibers. To do this, the films were placed between two identical metal masks having

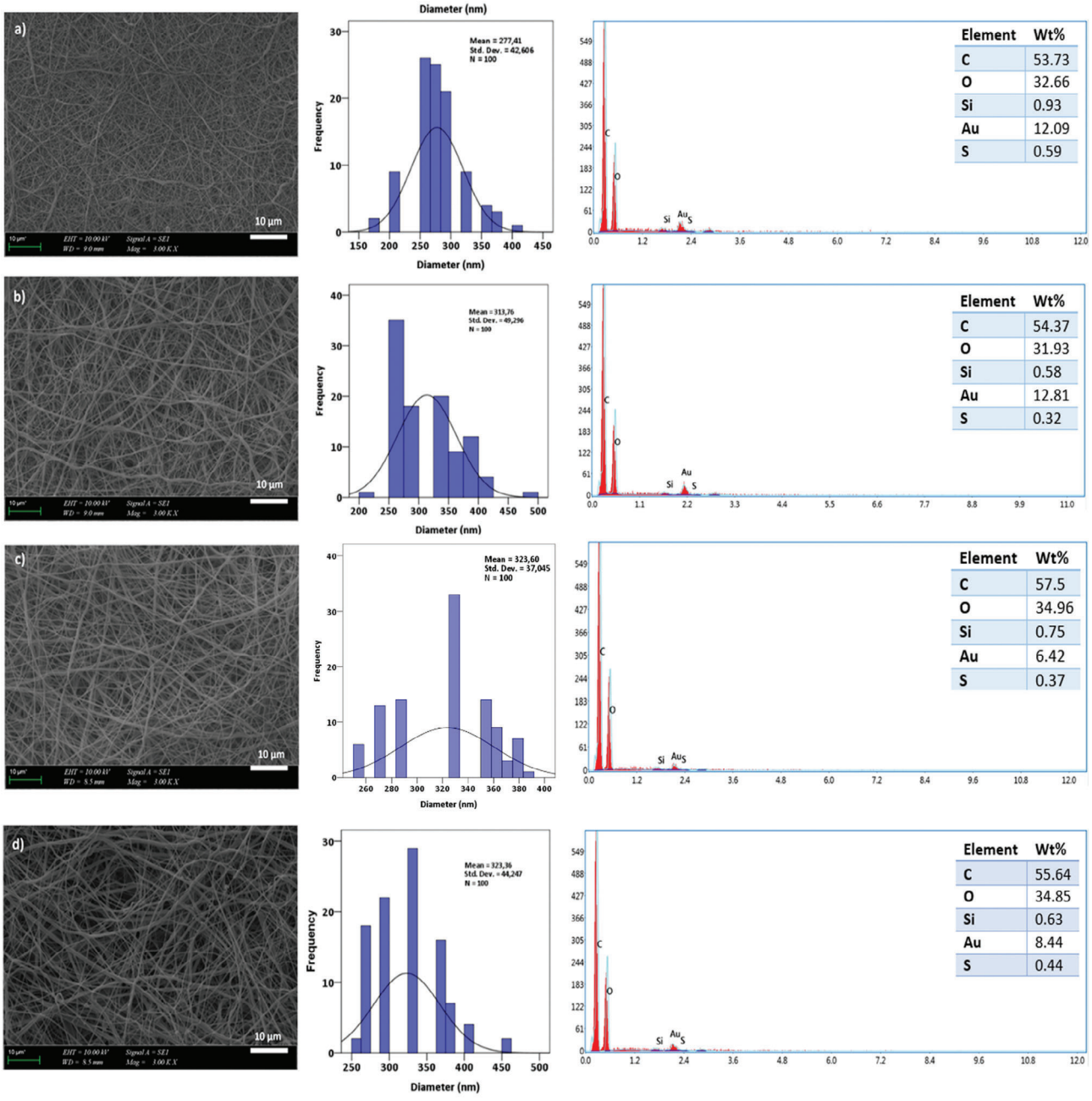

Figure 3. SEM images of the a) 17% PCL/1.5% GO, b) 17% PCL/1.5% GO/1% COL, c) 17% PCL/1.5% GO/3% COL, and d) 17% PCL/1.5% GO/5% COL nanofibers.

circular holes with a diameter of 4 mm. The metal masks were placed into a physical vapor deposition system. In high vacuum ambient ($<10^{-6}$ mbar), silver metal was evaporated on both sides of the films using a tungsten boat. Metal contacts to silver electrodes were performed by using silver paste.

3. Results and Discussions

Figure 2 shows the relevant peaks of the FT-IR spectra of all nanofibers. All spectra proved the presence of peaks at the wave number of ≈2900 $cm^{-1,}$ which shows the presence of stretching and vibration of —CH_2— functional groups associated with alkyl long chains. This peak, in addition to those observed at the wave numbers of ≈1100, ≈1200· and ≈1800 cm^{-1}, indicates the presence of ester bonds due to bands of O—C—O, C—O—C, and C—O, respectively.[31] These highlighted peaks represented the PCL spectra and were consistent with the literature.[31,32] Furthermore, in the spectra of (a), (b), and (c), the decoration with GO was highlighted with the band at the wavenumber of ≈1600 cm^{-1} that is typically ascribed to the C═C bond that is present in the

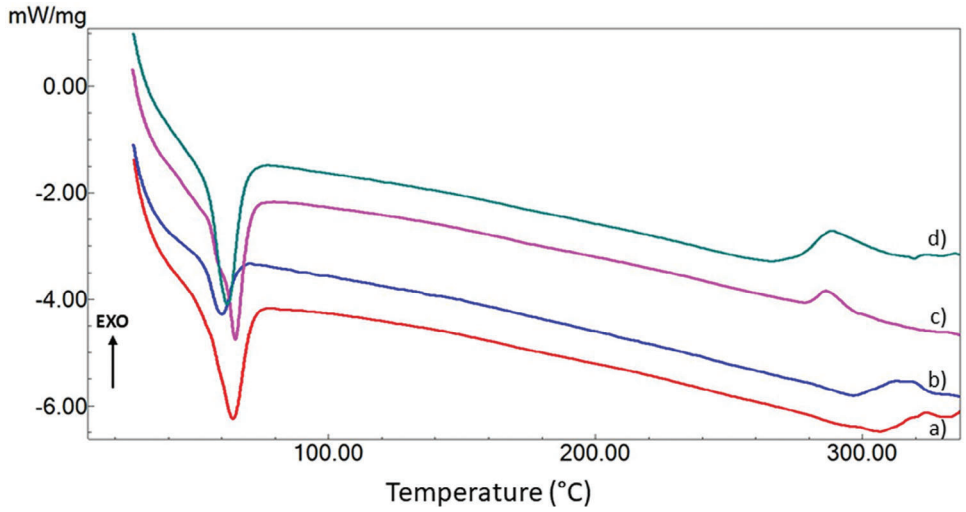

Figure 4. DSC curves of the nanofibers, a) 17% PCL/1.5% GO, b) 17% PCL/1.5% GO/1% COL, c) 17% PCL/1.5% GO/3% COL, and d) 17% PCL/1.5% GO/5% COL.

graphene lattice.[31] Similarly, the GO-related peaks at wavenumbers of 1750 and 1020 cm^{-1} due to C═O and C—O stretching vibration were also detected.[33] The absence of the traditional bands at the wavenumbers of 3500–3000 $cm^{-1,}$ which is typical for an O—H bond, was due to the higher overall FT-IR sensitivity of PCL compared to GO.[31] The intensity of bands presented at the wavenumbers of ≈1700 cm^{-1} and ≈1500–1600 cm^{-1} in spectra of (b), (c), and (d) also indicated the presence of amide I and amide II group functionalities.[34] The wavenumbers of the amide I group were due to vibration of the peptide C═O and stretching of C—N bonds, while the wavenumbers of amide II were due to N—H bending and some C—N stretching. Notably, the presence of the band at ≈1550 cm^{-1} indicates the presence of the triple helical structure of the COL.[34]

Figure 3 shows the morphologies of the nanofibers with mean pore diameters of 277.41 ± 42.6, 313.76 ± 49.2, 323.60 ± 37.04, and 323.36 ± 44.2 nm for 17% PCL/1.5% GO (a), 17% PCL/1.5% GO/1% COL (b), 17% PCL/1.5% GO/3% COL (c), and 17% PCL/1.5% GO/5% COL (d) nanofibers, respectively. Based on these values obtained by SEM, it was proven that the 17% PCL/1.5% GO nanofiber had the minimum pore diameter value. In contrast, the 17% PCL/1.5% GO/3% COL had the maximum pore diameter among the other nanofibers. On the other hand, no significant diameter difference was observed between the 17% PCL/1.5% GO/3% COL and 17% PCL/1.5% GO/5% COL nanofibers. Wenchao et al. fabricated PCL nanofibers by electrospinning method and found that 17% of PCL had nearly 211 nm pore diameter.[35] Atomic types and quantities of the surfaces of PCL-GO and PCL-GO-based COL nanofibers at different ratios were investigated using energy-dispersive X-ray spectroscopy (EDX) and SEM (Figure 3). The EDX spectra confirmed that the nanofibers do not contain atoms other than C, O, Au, S, and Si, determined in appropriate amounts. When the EDX spectra were inspected, it was seen that carbon (C) and oxygen (O) were present in very high proportions due to the presence of GO.[36] When the EDX spectra were investigated, it was seen that the highest C (57.5%) and O (34.96%) ratios belonged to the 17% PCL/1.5% GO/3% COL nanofibers.

DSC curves of the nanofibers containing different concentrations of PCL, COL, and GO can be used to determine the thermal properties of the composites (**Figure 4**). The DSC curves can show the individual components' melting points and the degree of interaction between them. The DSC curve of all nanofibers containing PCL with different concentrations of COL and GO showed a significant peak at around 60–70 °C, the melting peak of the PCL.[37] The melting peak of PCL is usually sharp and well-defined. The second peak, which appears as a shoulder in these C with 5% COL, is the melting point of the COL, which is usually around 40–60 °C.[38,39] This peak is due to the denaturation of the COL molecules. The DSC graph did not show the endothermic peak at around 220 °C, referring to the thermal decomposition of the oxygenated functional groups of the GO.[40] This can be due to the low content of GO in the composites.

XRD graphs of the PCL/GO and PCL/GO/COL nanofibers are given in **Figure 5**. Figure 5a represents the XRD peaks of the 17% PCL/1.5% GO nanofibers with their diffraction planes. As shown in Figure 5a, two sharp peaks were detected at $2\Theta = 21°$ (110) and 23.5° (200), which are the main XRD peaks of neat PCL. These peaks showed the semi-crystalline nature of the pure PCL.[41] Figure 5b–d represents the XRD peaks of the (1, 3, 5)% COL added 17% PCL nanofibers. The results showed that COL addition did not affect the main peaks of the 17% PCL/1.5% COL nanofibers significantly. According to the results, it can be said that the crystalline structure of 17% PCL/1.5% GO did not change with the addition of COL.

According to the results in **Table 1** and **Figure 6**, the 17% PCL/1.5% GO had a tensile strength value of 11.04 ± 1.11 MPa and 34.76 ± 4.55% elongation at break value. When 1% COL was added into the 17% PCL/1.5% GO nanofibers, it was observed that the tensile strength value of the 17% PCL/1.5% GO increased to the 11.45 ± 2.48 MPa and strain value increased sharply to the value of 53.72 ± 17.53%. On the other hand, with the addition of 3% COL into the 17% PCL/1.5% GO the tensile strength decreased to the value of 6.41 ± 0.53 MPa. In addition, the strain value also decreased to 53.72 ± 17.53%. By adding 5% COL into the 17% PCL/1.5% GO nanofiber, the tensile strength

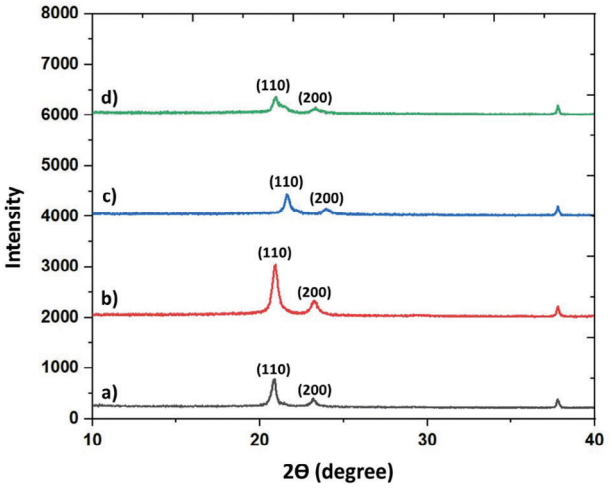

Figure 5. XRD graphs of the a) 17% PCL/1.5% GO, b) 17% PCL/1.5% GO/1% COL, c) 17% PCL/1.5% GO/3% COL, and d) 17% PCL/1.5% GO/5% COL nanofibers.

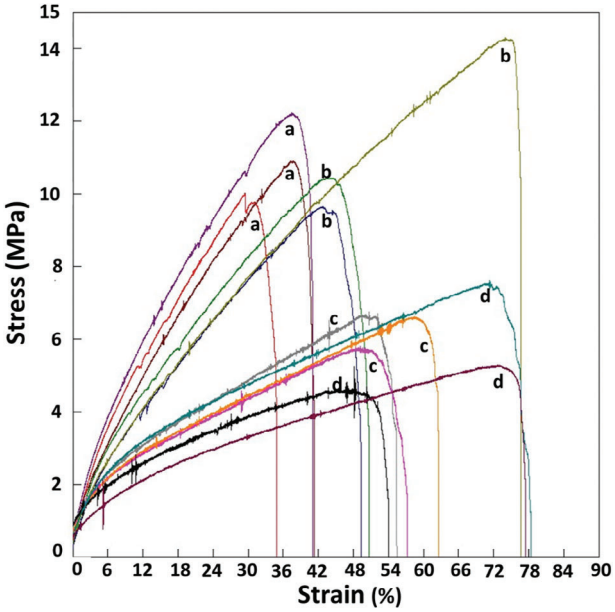

Figure 6. The stress versus strain graph of the nanofibers, a) 17% PCL/1.5% GO, b) 17% PCL/1.5% GO/1% COL, c) 17% PCL/1.5% GO/3% COL, and d) 17% PCL/1.5% GO/5% COL.

value again reduced to the value of 6.03 ± 1.35 MPa. However, the strain value increased again to the value of 64.12 ± 13.81%. Due to increasing the concentration of COL from 1 to 5%, we observed an increase in strain at break value as the COL could improve the polymer chain movement. The elongation at a break of 61% was reported for PCL: COL electrospun nanofibers,[42] which is close to the observed data in this study (Table 1). The Young's modulus values of the nanofibers were given in Table 1, and results showed that COL addition decreased the Young's modulus values of the 17% PCL/1.5% GO nanofibers. The modulus of elasticity is a value that indicates the stiffness of the material. The greater the modulus of elasticity, the more rigid the material.[43] In this study, it can be said that the addition of COL reduced the stiffness of the 17% PCL/1.5% GO nanofibers and caused flexibility.

The swelling behavior of nanofibers is one of the essential parameters widely tested in tissue engineering.[44] The swelling graph of PCL/GO-based electrospun nanofibers is given in **Figure 7**. PCL/GO nanofibers showed a noticeable change in structure with increasing COL content. As seen in Figure 7, an increase was observed in the liquid absorption of the composite structure along with the COL ratio. The minimum swelling rate belonged to the 17% PCL/1.5% GO/1% COL nanofibers during the incubation period. Although the highest swelling rate was found for 17%PCL/1.5%GO/3%COL nanofiber until the third day, after that time, the highest swelling rate was observed for 17%PCL/1.5%GO/5%COL nanofibers. According to the results, it can be said that the swelling rate of 17%PCL/1.5%GO nanofibers improved with the addition of a high COL amount. This is an important parameter because the swelling behavior is critical in the adhesion and proliferation of cells to the nanofibers. Therefore, controlling the swelling behavior of materials is vital, especially in dressing production.[45] The results proved that COL-doped PCL/GO nanofibers increased hydrophilicity and led to a better dressing interaction.

The viability of cardiomyocytes in the presence of the nanofibers was therefore assessed with the results presented in **Figure 8**. When the viability values were examined on the first day, it was observed that the cell viability was higher than the viability value of 17% PCL/1.5% GO nanofiber with the addition of 1% and 3% COL. The highest cell viability value (101.2%) for the first day was found in the 17% PCL/1.5%GO/1% COL nanofiber. On the third day of incubation, the cell viability values increased for all nanofibers, and the highest viability value (105.1%) was found for 17% PCL/1.5%GO/5% COL nanofibers. When the cell viability values taken on the seventh day were examined, it can be said that the cell viability values for all nanofibers decreased, and the highest viability value (84.8%) belonged to the PCL/1.5%GO/5% COL nanofibers. In all cases, the cell viability was >90% when exposed to the nanofibers for up to 3 days. The cells continued growth up to day 3, and then the proliferation decreased. This reduction of cell proliferation could be a consequence of the rapid cell proliferation on day 3, which resulted

Table 1. The mechanical properties of the nanofibers.

Fibers	Tensile strength [MPa]	Strain at break [%]	Young's modulus
17% PCL/1.5% GO	11.04 ± 1.11	34.76 ± 4.55	0.73 ± 0.088
17% PCL/1.5% GO/1% COL	11.45 ± 2.48	53.72 ± 17.53	0.57 ± 0.051
17% PCL/1.5% GO/3% COL	6.41 ± 0.53	52.09 ± 3.83	0.52 ± 0.017
17% PCL/1.5% GO/5% COL	6.03 ± 1.35	64.12 ± 13.81	0.44 ± 0.102

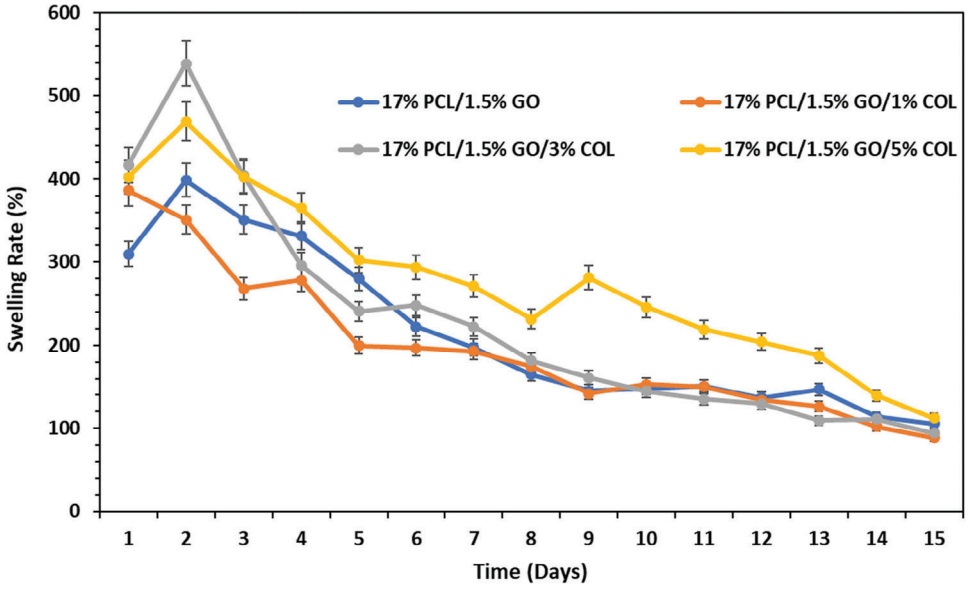

Figure 7. Swelling behaviors of the electrospun nanofibers.

in a crowded growth area and, consequently, a decline on day 7.[46] Heidari et al. observed a higher cell growth on graphene-incorporated PCL/gelatin composites compared to PCL/gelatin nanofibers, which could be related to the higher hydrophobicity of graphene-containing composites mainly associated with hydroxyl groups present in the structure of graphene.[47] The higher hydrophilicity of the composite improves cell proliferation attachment and adhesion; this may also lead to a higher capacity of the nanofiber to adsorb proteins. Cell fluorescence imaging was also consistent with the MTT assay, and cells continued to proliferate on the fibers (**Figure 9**). It should be noted that the PCL degradation rate is affected by the presence of oxygen and humidity in the environment, which may lead to the loss of cell viability. Therefore, careful consideration must be taken when selecting PCL for a particular application. **Figure 10** showed that COL scanning at different ratios to 17% PCL/1.5% GO significantly altered the

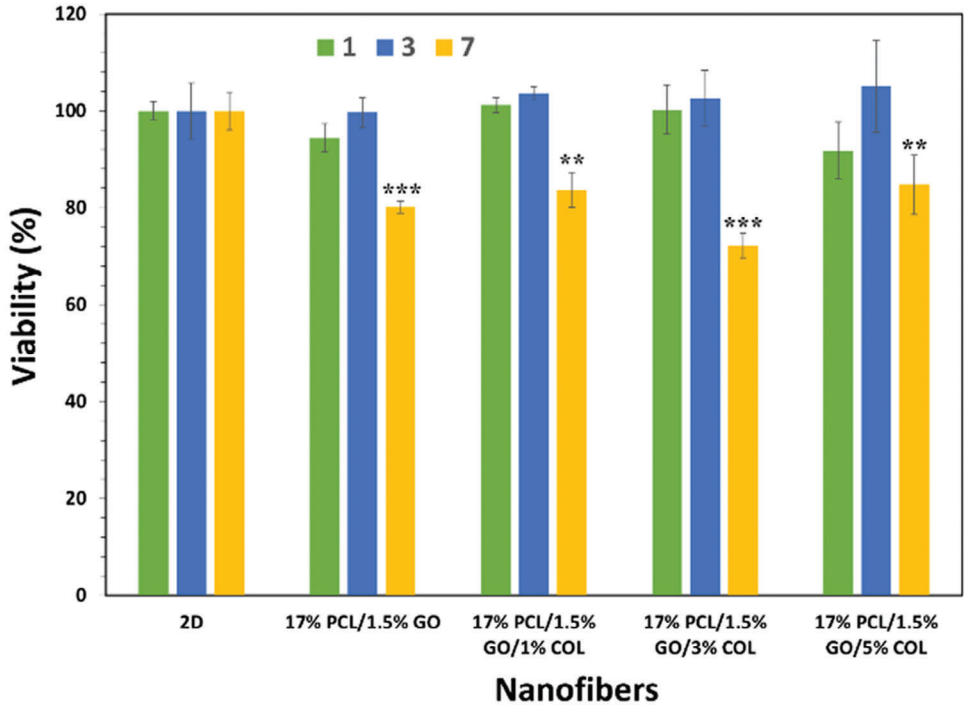

Figure 8. MTT assay of the nanofibers after 1, 3, and 7 days of the incubation period. Statistical significances were determined using one-way ANOVA Turkey Kramer multiple comparisons test compared to 2D. $^{**}p < 0.01$, and $^{***}p < 0.001$ show significance levels.

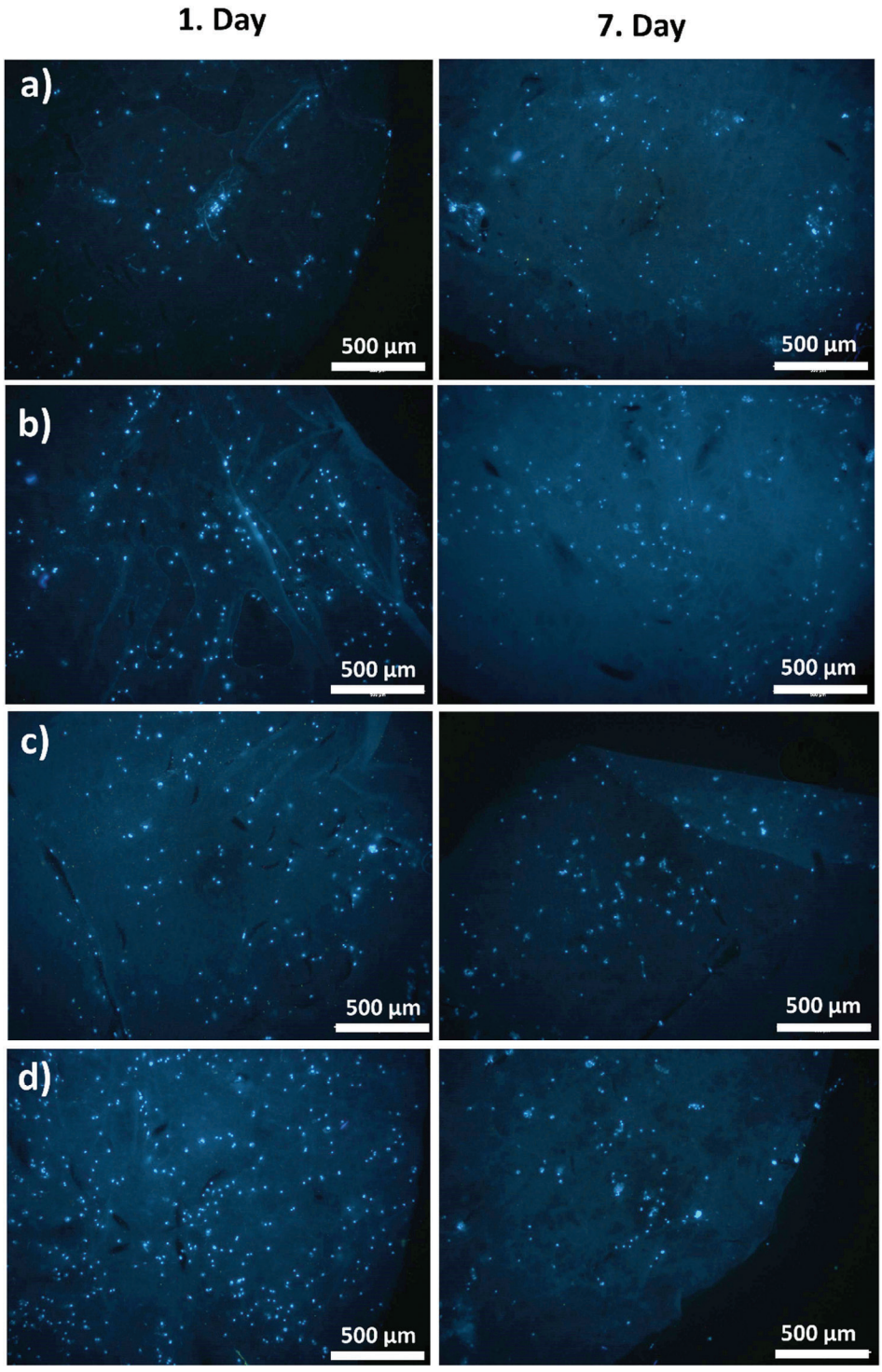

Figure 9. The fluorescent images of the cardiomyocytes on the a) 17% PCL/1.5% GO, b) 17% PCL/1.5% GO/1% COL, c) 17% PCL/1.5% GO/3% COL, and d) 17% PCL/1.5% GO/5% COL nanofibers.

morphological structure of cultured cardiomyocyte cells. However, the cell distribution in the 17% PCL/1.5% GO nanofiber was more regular spherical, and the cellular connectivity was higher than the others. When the cardiomyocyte growth on the seventh day was inspected, it was possible to see the morphological region as a clear and more distinct form. It can be said that cell proliferation in the structures of nanofibers in COL is more.

The thick films of the PCL/GO-based electrospun nanofibers with silver electrodes were placed in a vacuum chamber to measure DC and AC electrical parameters. DC conductivity

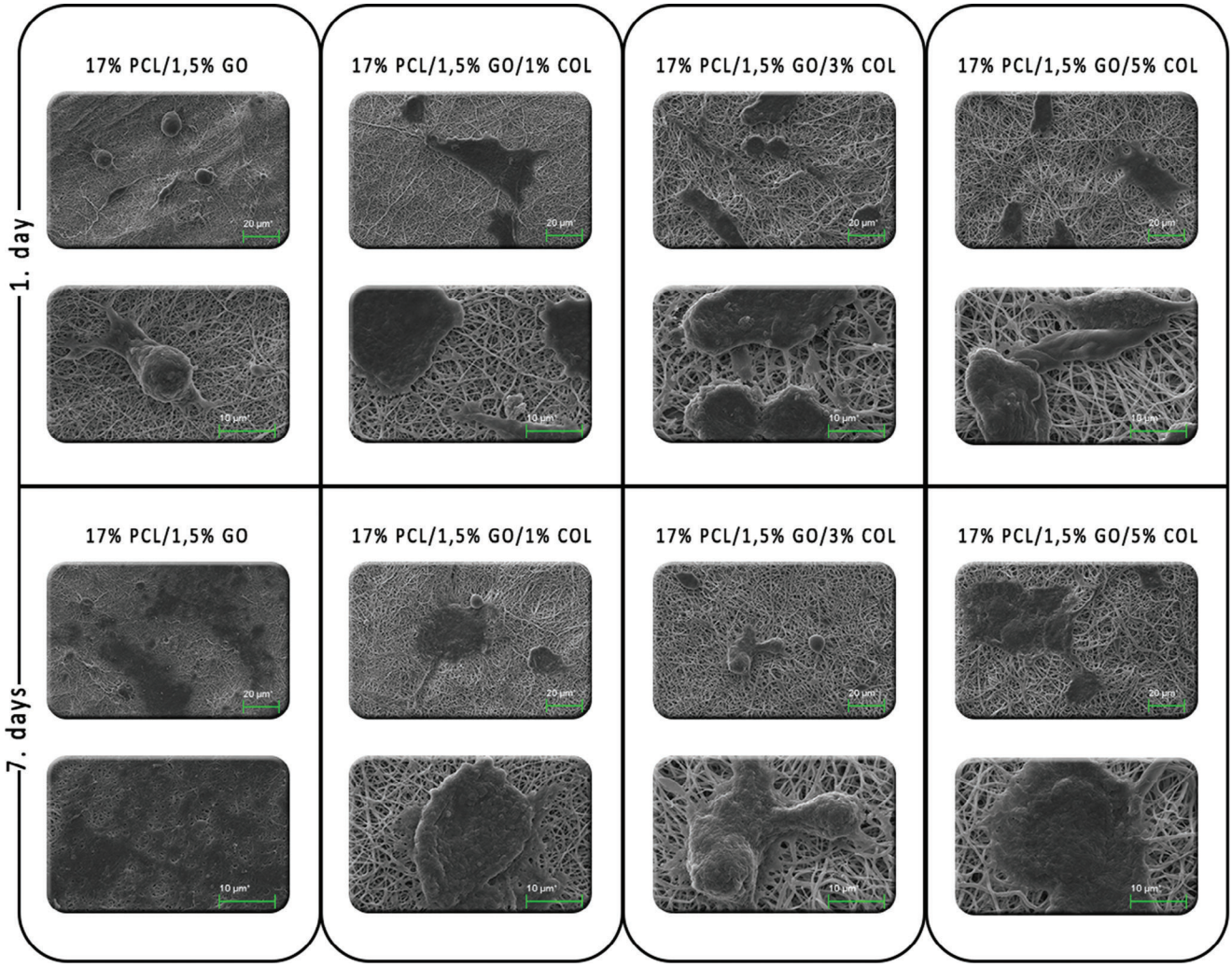

Figure 10. The SEM images of cardiomyocyte cells on nanofibers after 1 and 7 days of incubation time.

measurements were performed by applying DC voltages between −1 and 1 V with 0.1 V steps at 25 and 40 °C using a Keithley model 6517B electrometer. DC conductivity values of the films were calculated by using the slope of the *I*–*V* curves. **Figure 11** presented the *I*–*V* curves of the film of composite nanofiber 17% PCL/1.5% GO at 25 °C in a vacuum. *I*–*V* curves of the other films under investigation showed similar curves.

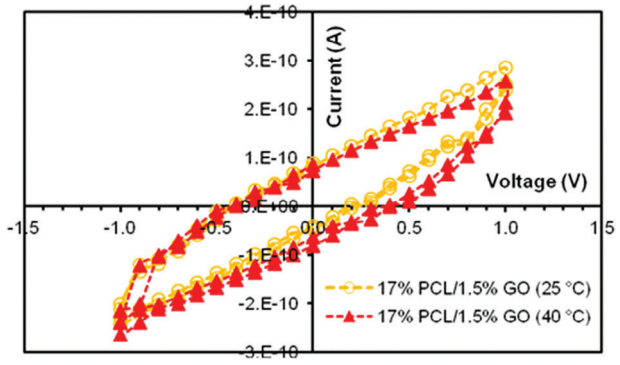

Figure 11. *I*–*V* curve of the film of composite nanofiber 17% PCL/1.5% GO in vacuum (10^{-3} mbar) at 25 and 40 °C.

As seen in Figure 11, the *I*–*V* curve showed ohmic behavior with hysteresis indicating traps in the band gap. The variation of calculated DC conductivity values as a function of COL contents is given in **Figure 12**.

By examining Figure 12, we obtained that an increase in COL content through 1 wt% DC conductivity values decreased than through 5 wt%, the values increased. We can conclude that increased COL content caused a limited change in the DC conductivity values of the films.

To investigate the temperature dependence of the films, DC conductivity measurements were also performed at an elevated temperature of 40 °C, a bit greater than the average body temperature. The results revealed that an increase in temperature caused an increase in the DC conductivity values of the films of nanofibers. Still, the results were found in the same range of the DC conductivity at 25 °C and 40 °C, 10^{-10} S m^{-1}.

The electrical response of the films was also investigated as a function of frequency. AC conductivity measurements were done in a vacuum ambient between 40 and 10^4 Hz at 25 and 40 °C

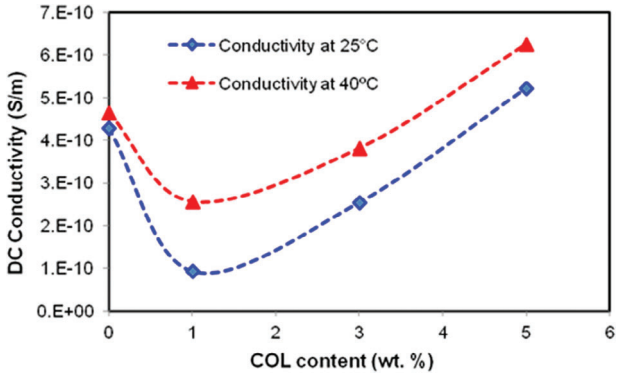

Figure 12. The variation of DC conductivity of the films versus COL content (wt%) in vacuum ambient (10^{-3} mbar) at 25 and 40 °C.

using Keithley model 3330 LCZ meter. **Figure 13** shows the variation of AC conductivity values of the films of nanofibers at 25 °C in vacuum.

As seen in Figure 13, AC conductivity values (σ_{AC}) of the film of 17% PCL/1.5% GO increased with increasing frequency and showed logarithmic behavior. This behavior can be represented by a power law (Equation (2)).

$$\sigma_{AC}(\omega) = a\omega^n \quad (2)$$

where ω is the applied voltage frequency, and a is the coefficient of ω. The frequency dependence of the AC conductivity of the films remained nearly the same; however, it tended to decrease at low frequencies. A similar behavior was observed for the films of 17% PCL/1.5% GO/1% COL, 17% PCL/1.5% GO/3% COL, and 17% PCL/1.5% GO/5% COL.

As in the case of DC conductivity measurements, to investigate the response of the films to AC signal at elevated temperatures, the AC conductivity measurements were done at 40 °C. **Figure 14** presented the AC conductivity of films of 17% PCL/1.5% GO and 17% PCL/1.5% GO/1% COL as a function of frequency at 25 °C and 40 °C to compare the AC response of the films.

From Figure 14, we may say that with the increase in temperature from 25 °C to 40 °C, there was no remarkable change in the AC conductivity values of the films investigated.

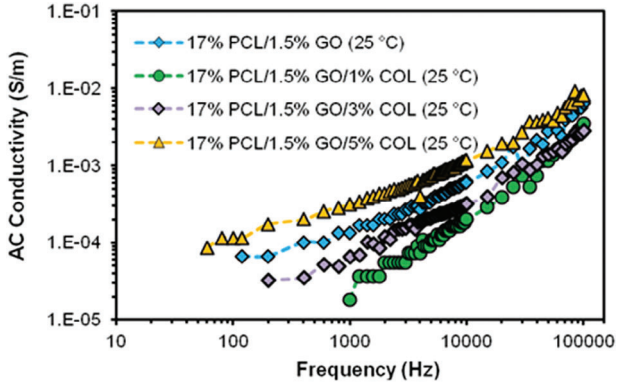

Figure 13. The frequency dependence of AC conductivity of the films of nanofibers with different COL contents in vacuum (10^{-3} mbar) at 25 °C.

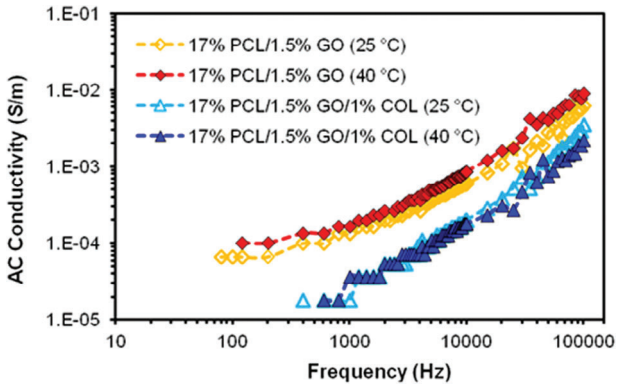

Figure 14. The frequency dependence of AC conductivity of the films of 17% PCL/1.5% GO and 17% PCL/1.5% GO/1% COL in vacuum (10^{-3} mbar) at indicated temperatures.

4. Conclusions

The homogeneous and bead-free nanofibers from PCL, GO, and COL were successfully fabricated using the electrospinning technique. The SEM results revealed that the addition of COL partially increased the diameter of the 17% PCL/1.5% GO fibers. The FTIR analysis showed the homogeneous distributions of the COL into the 17% PCL/1.5% GO fibers. The tensile test results of the fibers demonstrated that 1% COL addition increased the tensile strength value of the 17% PCL/1.5% GO fibers from 11.04 ± 1.11 MPa to 11.45 ± 2.48 MPa, but 3 and 5% COL addition decreased this value. The XRD results indicated that the addition of COL did not affect the crystalline structure of 17% PCL/1.5% GO fibers. The XRD spectrums proved that COL addition did not distribute the crystalline structure of the PCL/GO fibers. The biocompatibility test performed with cardiomyocytes showed that COL-added fibers showed more suitable conditions for cell survival.

Acknowledgements

This study was supported financially by TUBITAK 2209-A-Research Project Support Program for Undergraduate Students (project no: 1919B012212828) project. The authors also thank to Marmara University Scientific Research Committee (BAPKO Project Number: FYL-2022-10636) for their financial support.

Conflict of Interest

The authors declare no conflict of interest.

Author Contributions

S.U. and O.G. conceptualized the study. S.S.K., M.N.D., Z.A., and E.N.Y. were involved in the investigation process. S.U., A.Sa., F.D., and O.G. contributed to the development of the methodology. S.U. and O.G. provided supervision for the study. S.U., A.Sa., and O.G. were responsible for visualizing the data. O.V.O., L.N., A.S., S.U., and F.D. were involved in writing the original draft, and O.V.O., L.N., A.Sh., S.U., F.D., and O.G. actively contributed to the review and editing process.

Data Availability Statement

The data that support the findings of this study are available from the corresponding author upon reasonable request.

Keywords

collagen, conductivity, electrospinning, graphene oxide, myocardial tissue, nanofiber, polycaprolactone

Received: May 23, 2023
Revised: September 30, 2023
Published online:

[1] F. Ibrahim, A. Thiha, W. S. Wan Kamarul Zaman, Y. Kamarulzaman, N. A. Dahlan, N. F. Jamaluddin, M. J. Madou, *Mater. Today Commun.* **2022**, *33*, 104285.
[2] E. Pena-Mercado, C. Sanchez-Gomez, M. Garcia-Lorenzana, J. C. Ruiz, I. Arroyo-Maya, S. Huerta-Yepez, J. Campos-Teran, *Polymers* **2022**, *14*, 3233.
[3] M. O. Aydogdu, J. Chou, E. Altun, N. Ekren, S. Cakmak, M. Eroglu, A. A. Osman, O. Kutlu, E. T. Oner, G. Avsar, F. N. Oktar, I. Yilmaz, O. Gunduz, *Int. J. Polym. Mater. Polym. Biomater.* **2019**, *68*, 243.
[4] J. A. Roacho-Pérez, E. N. Garza-Treviño, N. K. Moncada-Saucedo, P. A. Carriquiry-Chequer, L. E. Valencia-Gómez, E. R. Matthews, V. Gómez-Flores, M. Simental-Mendía, P. Delgado-Gonzalez, J. L. Delgado-Gallegos, G. R. Padilla-Rivas, J. F. Islas, *Life* **2022**, *12*, 1117.
[5] U. Kaundal, U. Bagai, A. Rakha, *J. Transl. Med.* **2018**, *16*, 31.
[6] W. L. Stoppel, D. L. Kaplan, L. D. Black, *Adv. Drug Delivery Rev.* **2016**, *96*, 135.
[7] S. N. H. Karimi, R. M. Aghdam, S. A. S. Ebrahimi, Y. Chehrehsaz, *Polym. Int.* **2022**, *71*, 1099.
[8] S. Cesur, S. Ulag, L. Ozak, A. Gumussoy, S. Arslan, B. K. Yilmaz, N. Ekren, M. Agirbasli, D. M. Kalaskar, O. Gunduz, *Polym. Test.* **2020**, *90*, 106613.
[9] Q. Wang, H. Yang, A. Bai, W. Jiang, X. Li, X. Wang, Y. Mao, C. Lu, R. Qian, F. Guo, T. Ding, H. Chen, S. Chen, J. Zhang, C. Liu, N. Sun, *Biomaterials* **2016**, *105*, 52.
[10] A.-I. Lazar, K. Aghasoleimani, A. Semertsidou, J. Vyas, A.-L. Rosca, D. Ficai, A. Ficai, *Nanomaterials* **2023**, *13*, 1092.
[11] M. Zhang, Z. Li, P. Jiang, T. Lin, X. Li, D. Sun, *J. Appl. Polym. Sci.* **2017**, *134*, 45109.
[12] A. Hernández-Rangel, E. S. Martin-Martinez, *J. Biomed. Mater. Res., Part A* **2021**, *109*, 1751.
[13] Y. Dai, J. Ahmed, M. Edirisinghe, *Macromol. Mater. Eng.* **2023**, *308*, 2300033.
[14] R. Tarcan, O. Todor-Boer, I. Petrovai, C. Leordean, S. Astilean, I. Botiz, *J. Mater. Chem. C* **2020**, *8*, 1198.
[15] M. He, R. Zhang, K. Zhang, Y. Liu, Y. Su, Z. Jiang, *J. Mater. Chem. A* **2019**, *7*, 11468.
[16] W. Yu, L. Sisi, Y. Haiyan, L. Jie, *RSC Adv.* **2020**, *10*, 15328.
[17] E. Pinar, A. Sahin, S. Unal, O. Gunduz, F. Harman, E. Kaptanoglu, *Eur. Polym. J.* **2022**, *165*, 111000.
[18] A. B. Seabra, A. J. Paula, R. De Lima, O. L. Alves, N. Durán, *Chem. Res. Toxicol.* **2014**, *27*, 159.
[19] A.-M. Croitoru, Y. Karaçelebi, E. Saatcioglu, E. Altan, S. Ulag, H. K. Aydogan, A. Sahin, L. Motelica, O. Oprea, B.-M. Tihauan, R.-C. Popescu, D. Savu, R. Trusca, D. Ficai, O. Gunduz, A. Ficai, *Pharmaceutics* **2021**, *13*, 957.
[20] D. A. Samani, A. Doostmohammadi, M. R. Nilforoushan, H. Nazari, *Fibers Polym.* **2019**, *20*, 982.
[21] A.-M. Croitoru, A. Ficai, D. Ficai, R. Trusca, G. Dolete, E. Andronescu, S. C. Turculet, *Materials* **2020**, *13*, 1687.
[22] S. R. Shin, C. Zihlmann, M. Akbari, P. Assawes, L. Cheung, K. Zhang, V. Manoharan, Y. S. Zhang, M. Yüksekkaya, K.-T. Wan, M. Nikkhah, M. R. Dokmeci, X. (.S.). Tang, A. Khademhosseini, *Small* **2016**, *12*, 3677.
[23] S. Ulag, C. Kalkandelen, F. N. Oktar, M. Uzun, Y. M. Sahin, B. Karademir, S. Arslan, I. T. Ozbolat, M. Mahirogullari, O. Gunduz, *ChemistrySelect* **2019**, *4*, 2387.
[24] S. Ulag, C. Kalkandelen, T. Bedir, G. Erdemir, S. E. Kuruca, F. Dumludag, C. B. Ustundag, E. Rayaman, N. Ekren, B. Kilic, O. Gunduz, *Mater. Sci. Eng., B* **2020**, *261*, 114660.
[25] Y. Wu, L. Wang, B. Guo, P. X. Ma, *ACS Nano* **2017**, *11*, 5646.
[26] M. E. Mutlu, S. Ulag, M. Sengor, S. Daglilar, R. Narayan, O. Gunduz, *Mater. Lett.* **2021**, *305*, 130844.
[27] O. A. Majid, A. T. R. Fricker, D. A. Gregory, N. Davidenko, O. H. Cruz, R. J. Jabbour, T. J. Owen, P. Basnett, B. Lukasiewicz, M. Stevens, S. Best, R. Cameron, S. Sinha, S. E. Harding, I. Roy, *Front. Cardiovasc. Med.* **2020**, *7*, 192.
[28] Y. Fang, T. Zhang, Y. Song, W. Sun, *Biomed. Mater.* **2020**, *15*, 045003.
[29] K. Roshanbinfar, L. Vogt, B. Greber, S. Diecke, A. R. Boccaccini, T. Scheibel, F. B. Engel, *Adv. Funct. Mater.* **2018**, *28*, 1803951.
[30] A. Croitoru, O. Oprea, A. Nicoara, R. Trusca, M. Radu, I. Neacsu, D. Ficai, A. Ficai, E. Andronescu, *Medicina* **2019**, *55*, 230.
[31] A. Maio, M. Gammino, E. F. Gulino, B. Megna, P. Fara, R. Scaffaro, *ACS Appl. Polym. Mater.* **2020**, *2*, 4993.
[32] J. Krzaczkowska, Z. Fojud, M. Kozak, S. Jurga, *Acta Phys. Pol., A* **2005**, *108*, 187.
[33] A. Lipovka, R. Rodriguez, E. Bolbasov, P. Maryin, S. Tverdokhlebov, E. Sheremet, *Surf. Coat. Technol.* **2020**, *388*, 125560.
[34] K. H. Sizeland, K. A. Hofman, I. C. Hallett, D. E. Martin, J. Potgieter, N. M. Kirby, A. Hawley, S. T. Mudie, T. M. Ryan, R. G. Haverkamp, M. H. Cumming, *Materialia* **2018**, *3*, 90.
[35] W. Li, L. Shi, X. Zhang, K. Liu, I. Ullah, P. Cheng, *J. Appl. Polym. Sci.* **2018**, *135*, 45578.
[36] A. Alshahrani, M. S. Bin-Shuwaish, R. S. Al-Hamdan, T. Almohareb, A. M. Maawadh, M. Al Deeb, A. M. Alhenaki, T. Abduljabbar, F. Vohra, *J. Appl. Biomater. Funct. Mater.* **2020**, *18*, 1.
[37] J. In Kim, C. S. Kim, *Mater. Sci. Eng., C* **2018**, *91*, 824.
[38] J. Gross, *Science* **1964**, *143*, 960.
[39] Y. Sun, W.-L. Chen, S.-J. Lin, S.-H. Jee, Y.-F. Chen, L.-C. Lin, P. T. C. So, C.-Y. Dong, *Biophys. J.* **2006**, *91*, 2620.
[40] A. Hussein, S. Sarkar, D. Oh, K. Lee, B. Kim, *J. Appl. Polym. Sci.* **2016**, *133*, 43821.
[41] S. Ulag, C. Kalkandelen, T. Bedir, G. Erdemir, S. E. Kuruca, F. Dumludag, C. B. Ustundag, E. Rayaman, N. Ekren, B. Kilic, O. Gunduz, *Mater. Sci. Eng., B* **2020**, *261*, 114660.
[42] J. Hackett, T. Dang, E. Tsai, X. Cao, *Materials* **2010**, *3*, 3714.
[43] V. V. Rodaev, A. I. Tyurin, S. S. Razlivalova, V. V. Korenkov, Y. I. Golovin, *Polymers* **2021**, *13*, 3932.
[44] S. Unal, S. Arslan, T. Gokce, B. M. Atasoy, B. Karademir, F. N. Oktar, O. Gunduz, *Eur. Polym. J.* **2019**, *115*, 157.
[45] V. Trakoolwannachai, P. Kheolamai, S. Ummartyotin, *Composites, Part B* **2019**, *173*, 106974.
[46] T. Chang, H. Yin, X. Yu, L. Wang, L. Fan, J. H. Xin, H. Yu, *Colloids Surf., B* **2022**, *214*, 112480.
[47] M. Heidari, S. H. Bahrami, M. Ranjbar-Mohammadi, P. B. Milan, *Mater. Sci. Eng., C* **2019**, *103*, 109768.